Analysis of the semileptonic $\Lambda_b \to \Lambda \ell^+ \ell^-$ transition in the topcolor-assisted technicolor model

K. Azizi,[1,*] S. Kartal,[2,†] A. T. Olgun,[2,‡] and Z. Tavukoğlu[2,§]

[1]*Department of Physics, Doğuş University, Acıbadem-Kadıköy, 34722 İstanbul, Turkey*
[2]*Department of Physics, İstanbul University, Vezneciler, 34134 İstanbul, Turkey*

(Received 16 July 2013; published 15 October 2013)

We comparatively analyze the flavor-changing neutral current process of $\Lambda_b \to \Lambda \ell^+ \ell^-$ in the standard model as well as the topcolor-assisted technicolor model using the form factors calculated via light cone QCD sum rules in full theory. In particular, we calculate the decay width, branching ratio and lepton forward-backward asymmetry related to this decay channel. We compare the results of the topcolor-assisted technicolor model with those of the standard model and debate how the results of the topcolor-assisted technicolor model depart from the standard model predictions. We also compare our results on the branching ratio and differential branching ratio with recent experimental data provided by CDF and LHCb Collaborations.

DOI: 10.1103/PhysRevD.88.075007 PACS numbers: 12.60.−i, 12.60.Nz, 13.30.−a, 13.30.Ce

I. INTRODUCTION

The flavor-changing neutral current (FCNC) processes in the baryonic sector are promising tools in the indirect search for new physics (NP) effects, in addition to the direct searches at large hadron colliders. Hence, both experimental and phenomenological works devoted to the analysis of these channels receive special attention nowadays. The semileptonic FCNC decay of $\Lambda_b \to \Lambda \ell^+ \ell^-$ ($\ell = e, \mu, \tau$) is one of the most important transitions in this respect since a heavy quark with a light diquark combination of the Λ_b baryon makes this process significantly different than the B-meson decays. Experimentally, the CDF Collaboration at Fermilab first reported their observation of the semileptonic $\Lambda_b^0 \to \Lambda \mu^+ \mu^-$ decay, with a statistical significance of 5.8σ and 24 signal events at $\sqrt{s} = 1.96$ TeV, collected by the CDF II detector in 2011 [1]. They measured a branching ratio of $[1.73 \pm 0.42(\text{stat}) \pm 0.55(\text{syst})] \times 10^{-6}$ [1] in the muon channel. Recently, the LHCb Collaboration at CERN also reported their observation of $\Lambda_b^0 \to \Lambda \mu^+ \mu^-$ with a signal yield of 78 ± 12, collected by the LHCb detector, corresponding to an integrated luminosity of 1.0 fb^{-1} at $\sqrt{s} = 7$ TeV [2]. They measured a branching ratio of $[0.96 \pm 0.16(\text{stat}) \pm 0.13(\text{syst}) \pm 0.21(\text{norm})] \times 10^{-6}$ in the muon channel. So far, there has been no direct evidence for the NP effects beyond the standard model (SM) at present particle physics experiments. However, the ATLAS and CMS Collaborations at CERN reported their observations of a new particle like the SM Higgs boson with a mass of $\sim$125 GeV at a statistical significance of 5σ in 2012 [3,4]. Taking into consideration the above experimental progress and recent developments at the LHC, by increasing the center-of-mass energy, we hope we will be able to search for more FCNC decay processes as well as NP effects in the near future. Therefore, theoretical calculations for NP effects on the FCNC processes using different scenarios will be required for analysis of the experimental results.

In the present work, we analyze the semileptonic FCNC channel of $\Lambda_b \to \Lambda \ell^+ \ell^-$ in the topcolor-assisted technicolor (TC2) model. We calculate many parameters such as decay width, branching ratio and forward-backward asymmetry (FBA) and look for the difference between the results from those of the SM predictions. We also compare our results with the above-mentioned experimental data.

The technicolor (TC) mechanism provides us with an alternative explanation for the origin of masses of the electroweak gauge bosons $W^\pm$ and Z^0 [5]. Although the TC and extended TC models explain the flavor symmetry and electroweak symmetry breakings (EWSB), these models are unable to explain why the mass of the top quark is too large [6,7]. In topcolor models, however, the top quark involves a new strong interaction, spontaneously broken at some high energy scales but not confining. According to these models, the strong dynamics provides the formation of the top quark condensate $\bar{t}t$ which leads to a large dynamical mass for this quark, but with unnatural fine tuning [7,8]. Hence, a TC model containing a topcolor scenario (TC2 model) has been developed [6]. This model explains the electroweak and flavor symmetry breakings as well as the large mass of the top quark without unnatural fine tuning. This model also predicts the existence of top pions ($\pi_t^{0,\pm}$), the top Higgs (h_t^0) and the nonuniversal gauge boson (Z'); we are going to discuss the dependencies of the physical quantities defining the $\Lambda_b \to \Lambda \ell^+ \ell^-$ transition on the masses of these objects in this article. For more details of the TC2 model and some of its applications, see for instance [9–12] and references therein.

The outline of the article is as follows. In the next section, after briefly introducing the TC2 scenario we present the effective Hamiltonian of the transition under consideration, including Wilson coefficients as well as the

*kazizi@dogus.edu.tr
†sehban@istanbul.edu.tr
‡a.t.olgun@gmail.com
§z.tavukoglu@gmail.com

transition amplitude and matrix elements in terms of form factors. In Sec. III, we calculate the differential decay width in the TC2 model and numerically analyze the differential branching ratio, the branching ratio and the lepton forward-backward asymmetry and compare the obtained results with those of the SM as well as existing experimental data.

II. SEMILEPTONIC $\Lambda_b \to \Lambda \ell^+ \ell^-$ TRANSITION IN THE SM AND TOPCOLOR-ASSISTED TECHNICOLOR MODEL

In this section, first we give a brief overview of the TC2 model. Then we present the effective Hamiltonian in both the SM and TC2 model and show how the Wilson coefficients that enter the low energy effective Hamiltonian are changed in the TC2 model compared to the SM. We also present the transition matrix elements in terms of form factors in full QCD and calculate the transition amplitude of $\Lambda_b \to \Lambda \ell^+ \ell^-$ in both models.

A. The TC2 model

As we previously mentioned, the TC2 model creates an attractive scheme because it combines the TC interaction, which is responsible for the dynamical EWSB mechanism as an alternative to the Higgs scenario, and the topcolor interaction for the third generation at a scale ~ 1 TeV. This model provides an explanation of the electroweak and flavor symmetry breakings and also the large mass of the top quark. This model predicts a triplet of strongly coupled pseudo-Nambu-Goldstone bosons, neutral-charged top pions ($\pi_t^{0,\pm}$) near the top mass scale, one isospin-singlet boson, the neutral top Higgs (h_t^0) and the nonuniversal gauge boson (Z'). Exchange of these new particles generates flavor-changing (FC) effects which lead to changes in the Wilson coefficients compared to the SM [6].

The flavor-diagonal (FD) couplings of top pions to the fermions are defined as [6,7,13–15]

$$\frac{m_t^*}{\sqrt{2}F_\pi}\frac{\sqrt{\nu_w^2 - F_\pi^2}}{\nu_w}\Big[i\bar{t}\gamma^5 t\pi_t^0 + \sqrt{2}\bar{t}_R b_L \pi_t^+ + \sqrt{2}\bar{b}_L t_R \pi_t^-\Big] + \frac{m_b^*}{\sqrt{2}F_\pi}\Big[i\bar{b}\gamma^5 b\pi_t^0 + \sqrt{2}\bar{t}_L b_R \pi_t^+ + \sqrt{2}\bar{b}_R t_L \pi_t^-\Big] + \frac{m_l}{\nu}\bar{l}\gamma^5 l\pi_t^0, \tag{2.1}$$

where $m_t^* = m_t(1-\varepsilon)$ and $m_b^* = m_b - 0.1\varepsilon m_t$ denote the masses of the top and bottom quarks generated by topcolor interactions, respectively. Here, F_π is the physical top-pion decay constant which is estimated from the Pagels-Stokar formula, $\nu_w = \nu/\sqrt{2} = 174$ GeV, wherein the ν is defined as the vacuum expectation of the Higgs field and the factor $\frac{\sqrt{\nu_w^2 - F_\pi^2}}{\nu_w}$ represents the mixing effect between the Goldstone bosons (techni-pions) and top pions.

The FC couplings of top pions to the quarks can be written as [16–18]

$$\frac{m_t^*}{\sqrt{2}F_\pi}\frac{\sqrt{\nu_w^2 - F_\pi^2}}{\nu_w}[iK_{UR}^{tc}K_{UL}^{tt^*}\bar{t}_L c_R \pi_t^0 + \sqrt{2}K_{UR}^{tc^*}K_{DL}^{bb}\bar{c}_R b_L \pi_t^+ + \sqrt{2}K_{UR}^{tc}K_{DL}^{bb^*}\bar{b}_L c_R \pi_t^- + \sqrt{2}K_{UR}^{tc^*}K_{DL}^{ss}\bar{t}_R s_L \pi_t^+ + \sqrt{2}K_{UR}^{tc}K_{DL}^{ss^*}\bar{s}_L t_R \pi_t^-], \tag{2.2}$$

where $K_{UL(R)}$ and $K_{DL(R)}$ are rotation matrices that diagonalize the up-quark and down-quark mass matrices M_U and M_D for the down-type left- and right-hand quarks, respectively. The values of the coupling parameters are given as

$$K_{UL}^{tt} \approx K_{DL}^{bb} \approx K_{DL}^{ss} \approx 1, \qquad K_{UR}^{tc} \leq \sqrt{2\varepsilon - \varepsilon^2}. \tag{2.3}$$

The FD couplings of the new gauge boson Z' to the fermions are also given by [6,7,13–16]

$$\mathcal{L}_{Z'}^{FD} = -\sqrt{4\pi K_1}\Big\{Z'_\mu\Big[\frac{1}{2}\bar{\tau}_L\gamma^\mu\tau_L - \bar{\tau}_R\gamma^\mu\tau_R + \frac{1}{6}\bar{t}_L\gamma^\mu t_L + \frac{1}{6}\bar{b}_L\gamma^\mu b_L + \frac{2}{3}\bar{t}_R\gamma^\mu t_R - \frac{1}{3}\bar{b}_R\gamma^\mu b_R\Big] - \tan^2\theta' Z'_\mu\Big[\frac{1}{6}\bar{s}_L\gamma^\mu s_L - \frac{1}{3}\bar{s}_R\gamma^\mu s_R - \frac{1}{2}\bar{\mu}_L\gamma^\mu\mu_L - \bar{\mu}_R\gamma^\mu\mu_R - \frac{1}{2}\bar{e}_L\gamma^\mu e_L - \bar{e}_R\gamma^\mu e_R\Big]\Big\}, \tag{2.4}$$

where K_1 is the coupling constant taken in the region (0.3–1), θ' is the mixing angle and $\tan\theta' = \frac{g_1}{\sqrt{4\pi K_1}}$, with g_1 being the ordinary hypercharge gauge coupling constant.

The FC couplings of the nonuniversal Z' gauge boson to the fermions can be written as [19]

$$\mathcal{L}_{Z'}^{FC} = -\frac{g_1}{2}\cot\theta' Z'^\mu\Big\{\frac{1}{3}D_L^{bb}D_L^{bs*}\bar{s}_L\gamma_\mu b_L - \frac{2}{3}D_R^{bb}D_R^{bs*}\bar{s}_R\gamma_\mu b_R + \text{H.c.}\Big\}, \tag{2.5}$$

where D_L and D_R are matrices rotating the weak eigenbasis to the mass ones for down-type left- and right-hand quarks, respectively.

B. The effective Hamiltonian and Wilson coefficients

The $\Lambda_b \to \Lambda \ell^+ \ell^-$ decay is governed by the $b \to s\ell^+\ell^-$ transition at quark level in the SM, whose effective Hamiltonian is given by [20–23]

$$\mathcal{H}_{\text{SM}}^{\text{eff}} = \frac{G_F\alpha_{em}V_{tb}V_{ts}^*}{2\sqrt{2}\pi}[C_9^{\text{eff}}\bar{s}\gamma_\mu(1-\gamma_5)b\bar{\ell}\gamma^\mu\ell + C_{10}\bar{s}\gamma_\mu(1-\gamma_5)b\bar{\ell}\gamma^\mu\gamma_5\ell - 2m_b C_7^{\text{eff}}\frac{1}{q^2}\bar{s}i\sigma_{\mu\nu}q^\nu(1+\gamma_5)b\bar{\ell}\gamma^\mu\ell], \tag{2.6}$$

where G_F is the Fermi coupling constant, α_{em} is the fine structure constant, V_{tb} and V_{ts}^* are elements of the Cabibbo-Kobayashi-Maskawa matrix, q^2 is the transferred momentum squared, and $C_7^{\rm eff}$, $C_9^{\rm eff}$, C_{10} are the Wilson coefficients. Our main task in the following is to present the expressions of the Wilson coefficients. The Wilson coefficient $C_7^{\rm eff}$ in the leading log approximation in the SM is given by [24–27]

$$C_7^{\rm eff}(\mu_b) = \eta^{\frac{16}{23}} C_7(\mu_W) + \frac{8}{3}(\eta^{\frac{14}{23}} - \eta^{\frac{16}{23}}) C_8(\mu_W) + C_2(\mu_W) \sum_{i=1}^{8} h_i \eta^{a_i}, \tag{2.7}$$

where

$$\eta = \frac{\alpha_s(\mu_W)}{\alpha_s(\mu_b)} \tag{2.8}$$

and

$$\alpha_s(x) = \frac{\alpha_s(m_Z)}{1 - \beta_0 \frac{\alpha_s(m_Z)}{2\pi} \ln(\frac{m_Z}{x})}, \tag{2.9}$$

with $\alpha_s(m_Z) = 0.118$ and $\beta_0 = \frac{23}{3}$. The remaining functions in Eq. (2.7) are written as

$$\begin{aligned} C_7(\mu_W) &= -\frac{1}{2} D_0'^{\rm SM}(x_t), \\ C_8(\mu_W) &= -\frac{1}{2} E_0'^{\rm SM}(x_t), \\ C_2(\mu_W) &= 1, \end{aligned} \tag{2.10}$$

where the functions $D_0'^{\rm SM}(x_t)$ and $E_0'^{\rm SM}(x_t)$ with $x_t = \frac{m_t^2}{m_W^2}$ are given by

$$D_0'^{\rm SM}(x_t) = -\frac{(8x_t^3 + 5x_t^2 - 7x_t)}{12(1-x_t)^3} + \frac{x_t^2(2-3x_t)}{2(1-x_t)^4} \ln x_t \tag{2.11}$$

and

$$E_0'^{\rm SM}(x_t) = -\frac{x_t(x_t^2 - 5x_t - 2)}{4(1-x_t)^3} + \frac{3x_t^2}{2(1-x_t)^4} \ln x_t. \tag{2.12}$$

The coefficients h_i and a_i in Eq. (2.7), with i running from 1 to 8, are also given by [25,26]

$$h_i = \left(2.2996, \quad -1.0880, \quad -\frac{3}{7}, \quad -\frac{1}{14}, \quad -0.6494, \quad -0.0380, \quad -0.0186, \quad -0.0057\right) \tag{2.13}$$

and

$$a_i = \left(\frac{14}{23}, \quad \frac{16}{23}, \quad \frac{6}{23}, \quad -\frac{12}{23}, \quad 0.4086, \quad -0.4230, \quad -0.8994, \quad 0.1456\right). \tag{2.14}$$

The Wilson coefficient $C_9^{\rm eff}$ in the SM is expressed as [25,26]

$$\begin{aligned} C_9^{\rm eff}(\hat{s}') = {} & C_9^{\rm NDR} \eta(\hat{s}') + h(z,\hat{s}')(3C_1 + C_2 + 3C_3 + C_4 \\ & + 3C_5 + C_6) - \frac{1}{2} h(1,\hat{s}')(4C_3 + 4C_4 + 3C_5 + C_6) \\ & - \frac{1}{2} h(0,\hat{s}')(C_3 + 3C_4) + \frac{2}{9}(3C_3 + C_4 + 3C_5 + C_6), \end{aligned} \tag{2.15}$$

where $\hat{s}' = \frac{q^2}{m_b^2}$ with q^2 in the interval $4m_l^2 \le q^2 \le (m_{\Lambda_b} - m_\Lambda)^2$. The $C_9^{\rm NDR}$ in the naive dimensional regularization (NDR) scheme is given as

$$C_9^{\rm NDR} = P_0^{\rm NDR} + \frac{Y^{\rm SM}}{\sin^2\theta_W} - 4Z^{\rm SM} + P_E E^{\rm SM}, \tag{2.16}$$

where $P_0^{\rm NDR} = 2.60 \pm 0.25$, $\sin^2\theta_W = 0.23$, $Y^{\rm SM} = 0.98$ and $Z^{\rm SM} = 0.679$ [25–27]. The last term in Eq. (2.16) is ignored due to the smallness of the value of P_E. The $\eta(\hat{s}')$ in Eq. (2.15) is also defined as

$$\eta(\hat{s}') = 1 + \frac{\alpha_s(\mu_b)}{\pi} \omega(\hat{s}'), \tag{2.17}$$

with

$$\begin{aligned} \omega(\hat{s}') = {} & -\frac{2}{9}\pi^2 - \frac{4}{3}\mathrm{Li}_2(\hat{s}') - \frac{2}{3}\ln\hat{s}'\ln(1-\hat{s}') \\ & - \frac{5+4\hat{s}'}{3(1+2\hat{s}')}\ln(1-\hat{s}') - \frac{2\hat{s}'(1+\hat{s}')(1-2\hat{s}')}{3(1-\hat{s}')^2(1+2\hat{s}')} \\ & \times \ln\hat{s}' + \frac{5+9\hat{s}'-6\hat{s}'^2}{6(1-\hat{s}')(1+2\hat{s}')}. \end{aligned} \tag{2.18}$$

The function $h(y,\hat{s}')$ is given as

$$h(y,\hat{s}') = -\frac{8}{9}\ln\frac{m_b}{\mu_b} - \frac{8}{9}\ln y + \frac{8}{27} + \frac{4}{9}x \tag{2.19}$$

$$-\frac{2}{9}(2+x) |1-x|^{1/2} \begin{cases} \left(\ln\left|\frac{\sqrt{1-x}+1}{\sqrt{1-x}-1}\right| - i\pi\right) & \text{for } x \equiv \frac{4z^2}{\hat{s}'} < 1 \\ 2\arctan\frac{1}{\sqrt{x-1}} & \text{for } x \equiv \frac{4z^2}{\hat{s}'} > 1, \end{cases} \tag{2.20}$$

where $y = 1$ or $y = z = \frac{m_c}{m_b}$ and

$$h(0,\hat{s}') = \frac{8}{27} - \frac{8}{9}\ln\frac{m_b}{\mu_b} - \frac{4}{9}\ln\hat{s}' + \frac{4}{9}i\pi. \tag{2.21}$$

At the $\mu_b = 5$ GeV scale, the coefficients C_j $(j = 1,\ldots,6)$ are given by [27]

$$C_j = \sum_{i=1}^{8} k_{ji}\eta^{a_i} \qquad (j = 1,\ldots,6), \tag{2.22}$$

where the constants k_{ji} are given as

$$\begin{aligned}
k_{1i} &= \left(0,\ 0,\ \tfrac{1}{2},\ -\tfrac{1}{2},\ 0,\ 0,\ 0,\ 0,\right),\\
k_{2i} &= \left(0,\ 0,\ \tfrac{1}{2},\ \tfrac{1}{2},\ 0,\ 0,\ 0,\ 0,\right),\\
k_{3i} &= \left(0,\ 0,\ -\tfrac{1}{14},\ \tfrac{1}{6},\ 0.0510,\ -0.1403,\ -0.0113,\ 0.0054\right),\\
k_{4i} &= \left(0,\ 0,\ -\tfrac{1}{14},\ -\tfrac{1}{6},\ 0.0984,\ 0.1214,\ 0.0156,\ 0.0026\right),\\
k_{5i} &= \left(0,\ 0,\ 0,\ 0,\ -0.0397,\ 0.0117,\ -0.0025,\ 0.0304\right),\\
k_{6i} &= \left(0,\ 0,\ 0,\ 0,\ 0.0335,\ 0.0239,\ -0.0462,\ -0.0112\right).
\end{aligned} \tag{2.23}$$

The Wilson coefficient C_{10} in the SM is scale independent and has the following explicit expression:

$$C_{10} = -\frac{Y^{\rm SM}}{\sin^2\theta_W}. \tag{2.24}$$

The effective Hamiltonian for the $b \to s\ell^+\ell^-$ transition in the TC2 model is given by [12]

$$\begin{aligned}
\mathcal{H}^{\rm eff}_{\rm TC2} = \frac{G_F\alpha_{em}V_{tb}V^*_{ts}}{2\sqrt{2}\pi}[&\tilde{C}_9^{\rm eff}\bar{s}\gamma_\mu(1-\gamma_5)b\bar{\ell}\gamma^\mu\ell\\
&+ \tilde{C}_{10}\bar{s}\gamma_\mu(1-\gamma_5)b\bar{\ell}\gamma^\mu\gamma_5\ell\\
&- 2m_b\tilde{C}_7^{\rm eff}\frac{1}{q^2}\bar{s}i\sigma_{\mu\nu}q^\nu(1+\gamma_5)b\bar{\ell}\gamma^\mu\ell\\
&+ C_{Q_1}\bar{s}(1+\gamma_5)b\bar{\ell}\ell + C_{Q_2}\bar{s}(1+\gamma_5)b\bar{\ell}\gamma_5\ell],
\end{aligned} \tag{2.25}$$

where $\tilde{C}_7^{\rm eff}$, $\tilde{C}_9^{\rm eff}$, $\tilde{C}_{10}$, C_{Q_1} and C_{Q_2} are new Wilson coefficients. $\tilde{C}_7^{\rm eff}$, $\tilde{C}_9^{\rm eff}$ and $\tilde{C}_{10}$ contain contributions from both the SM and TC2 model. The charged top pions $\pi_t^\pm$ only give contributions to the Wilson coefficient $\tilde{C}_7^{\rm eff}$, while the nonuniversal gauge boson Z' contributes to the Wilson coefficients $\tilde{C}_9^{\rm eff}$ and $\tilde{C}_{10}$. In the following, we present the explicit expressions of the Wilson coefficients $C_7(\mu_W)$ and $C_8(\mu_W)$ that enter Eq. (2.7) in the TC2 model. The new photonic- and gluonic-penguin diagrams in the TC2 model can be obtained by replacing the internal $W^\pm$ lines in SM penguin diagrams with unit-charged scalar ($\pi_1^\pm$, $\pi_8^\pm$ and $\pi_t^\pm$) lines (for more information, see Ref. [9]). As a result, the Wilson coefficients $\tilde{C}_7(\mu_W)$ and $\tilde{C}_8(\mu_W)$ in TC2 take the following forms [12,28]:

$$\begin{aligned}
\tilde{C}_7(\mu_W) &= -\frac{1}{2}D_0'^{\,\rm TC2tot}(x_t,z_t),\\
\tilde{C}_8(\mu_W) &= -\frac{1}{2}E_0'^{\,\rm TC2tot}(x_t,z_t),
\end{aligned} \tag{2.26}$$

where

$$\begin{aligned}
D_0'^{\,\rm TC2tot}(x_t,z_t) &= D_0'^{\,\rm SM}(x_t) + D_0'^{\,\rm TC2}(z_t),\\
E_0'^{\,\rm TC2tot}(x_t,z_t) &= E_0'^{\,\rm SM}(x_t) + E_0'^{\,\rm TC2}(z_t),
\end{aligned} \tag{2.27}$$

and

$$\begin{aligned}
D_0'^{\,\rm TC2}(z_t) &= \frac{1}{8\sqrt{2}G_FF_\pi^2}\Big[-\frac{22-53z_t+25z_t^2}{18(1-z_t)^3}\\
&\quad -\frac{3z_t-8z_t^2+4z_t^3}{3(1-z_t)^4}\log[z_t]\Big],\\
E_0'^{\,\rm TC2}(z_t) &= \frac{1}{8\sqrt{2}G_FF_\pi^2}\Big[-\frac{5-19z_t+20z_t^2}{6(1-z_t)^3}\\
&\quad +\frac{z_t^2-2z_t^3}{(1-z_t)^4}\log[z_t]\Big],
\end{aligned} \tag{2.28}$$

with $z_t = m_t^{*2}/m^2_{\pi_t^\pm}$.

There are new contributions coming from the nonuniversal gauge boson Z' in the TC2 model to the $Y^{\rm SM}$ and $Z^{\rm SM}$ that enter the $C_9^{\rm NDR}$ in Eq. (2.15) [12]. The $\tilde{C}_9^{\rm NDR}$ in the TC2 model is given by

$$\tilde{C}_9^{\rm NDR} = P_0^{\rm NDR} + \frac{Y^{\rm TC2tot}(y_t)}{\sin^2\theta_W} - 4Z^{\rm TC2tot}(y_t), \tag{2.29}$$

where

$$\begin{aligned}
Y^{\rm TC2tot}(y_t) &= Y^{\rm SM} + Y^{\rm TC2}(y_t),\\
Z^{\rm TC2tot}(y_t) &= Z^{\rm SM} + Z^{\rm TC2}(y_t).
\end{aligned} \tag{2.30}$$

The functions $Y^{\rm TC2}(y_t)$ and $Z^{\rm TC2}(y_t)$ are given by the following expressions in the case of e or μ in the final state [11,12]:

$$\begin{aligned}
Y^{\rm TC2}(y_t) &= Z^{\rm TC2}(y_t)\\
&= \frac{-\tan^2\theta' M_Z^2}{M_{Z'}^2}[K_{ab}(y_t) + K_c(y_t) + K_d(y_t)],
\end{aligned} \tag{2.31}$$

with $y_t = m_t^{*2}/m_W^2$. In the case of τ as a final leptonic state, the factor $-\tan^2\theta'$ in the above equation is replaced by 1. The functions in Eq. (2.31) are also defined as [29]

$$\begin{aligned}
K_{ab}(y_t) &= \frac{8}{3}(\tan^2\theta' - 1)\frac{F_1(y_t)}{(v_d + a_d)},\\
K_c(y_t) &= \frac{16F_2(y_t)}{3(v_u - a_u)} - \frac{8F_3(y_t)}{3(v_u + a_u)},\\
K_d(y_t) &= \frac{16F_4(y_t)}{3(v_u - a_u)} + \frac{8F_5(y_t)}{3(v_u + a_u)},
\end{aligned} \tag{2.32}$$

where

$$F_1(y_t) = -[0.5(Q-1)\sin^2\theta_W + 0.25]\{y_t^2\ln(y_t)/(y_t-1)^2 - y_t/(y_t-1) - y_t[0.5(-0.5772 + \ln(4\pi) - \ln(M_W^2)) + 0.75 - 0.5(x^2\ln(y_t)/(y_t-1)^2 - 1/(y_t-1))]\}[(1+y_t)/(y_t-2)],$$
$$F_2(y_t) = (0.5Q\sin^2\theta_W - 0.25)[y_t^2\ln(y_t)/(y_t-1)^2 - 2y_t\ln(y_t)/(y_t-1)^2 + y_t/(y_t-1)],$$
$$F_3(y_t) = -Q\sin^2\theta_W[y_t/(y_t-1) - y_t\ln(y_t)/(y_t-1)^2],$$
$$F_4(y_t) = 0.25(4\sin^2\theta_W/3 - 1)[y_t^2\ln(y_t)/(y_t-1)^2 - y_t - y_t/(y_t-1)],$$
$$F_5(y_t) = -0.25Q\sin^2\theta_W y_t[-0.5772 + \ln(4\pi) - \ln(M_W^2) + 1 - y_t ln(y_t)/(y_t-1)] - \sin^2\theta_W/6[y_t^2\ln(y_t)/(y_t-1)^2 - y_t - y_t/(y_t-1)], \quad (2.33)$$

and $a_{u,d} = I_3$, $v_{u,d} = I_3 - 2Q_{u,d}\sin^2\theta_W$, with u and d representing the up- and down-type quarks, respectively.

The Wilson coefficients C_{Q_1} and C_{Q_2} that appear in the effective Hamiltonian in the TC2 model belong to the neutral top pion π_t^0 and top Higgs h_t^0 contributing to the rare decays. The coefficient C_{Q_1} in the TC2 model is given by [11]

$$C_{Q_1} = \frac{\sqrt{v_w^2 - F_\pi^2}}{v_w}\left(\frac{m_b^* m_l v}{2\sqrt{2}\sin^2\theta_w F_\pi m_{h_t^0}^2}C_0(x_t) + \frac{V_{ts}m_l m_t m_b^{*2} M_W^2}{4\sqrt{2}g_2^4 F_\pi^2 m_{h_t^0}^2}C(x_s)\right), \quad (2.34)$$

where the Inami-Lim function $C_0(x_t)$ is defined by [27]

$$C_0(x_t) = \frac{x_t}{8}\left[\frac{x_t-6}{x_t-1} + \frac{3x_t+2}{(x_t-1)^2}\ln x_t\right]. \quad (2.35)$$

The $C(x_s)$ function in Eq. (2.34) is also given as [12]

$$C(x_s) = \frac{F_6(x)}{-[0.5(Q-1)\sin^2\theta_W + 0.25]}, \quad (2.36)$$

with

$$F_6(x_s) = -[0.5(Q-1)\sin^2\theta_W + 0.25]\{x_s^2\ln(x_s)/(x_s-1)^2 - x_s/(x_s-1) - x_s[0.5(-0.5772 + \ln(4\pi) - \ln(M_W^2)) + 0.75 - 0.5(x^2\ln(x_s)/(x_s-1)^2 - 1/(x_s-1))]\}, \quad (2.37)$$

where $x_s = m_t^{*2}/m_{\pi_t^0}^2$ and g_2 is the $SU(2)$ coupling constant. Since, the neutral top-Higgs coupling with fermions differs from that of the neutral top pion by a factor of γ_5, the form of C_{Q_2} is the same as C_{Q_1} except for the masses of the scalar particles [11].

C. Transition amplitude and matrix elements

The transition amplitude for the $\Lambda_b \to \Lambda\ell^+\ell^-$ decay is obtained by sandwiching the effective Hamiltonian between the initial and final baryonic states,

$$\mathcal{M}^{\Lambda_b\to\Lambda\ell^+\ell^-} = \langle\Lambda(p_\Lambda) \mid \mathcal{H}^{\rm eff} \mid \Lambda_b(p_{\Lambda_b})\rangle, \quad (2.38)$$

where p_{Λ_b} and p_Λ are momenta of the Λ_b and Λ baryons, respectively. In order to calculate the transition amplitude, we need to define the following matrix elements in terms of twelve form factors in full QCD:

$$\langle\Lambda(p_\Lambda) \mid \bar{s}\gamma_\mu(1-\gamma_5)b \mid \Lambda_b(p_{\Lambda_b})\rangle = \bar{u}_\Lambda(p_\Lambda)[\gamma_\mu f_1(q^2) + i\sigma_{\mu\nu}q^\nu f_2(q^2) + q^\mu f_3(q^2) - \gamma_\mu\gamma_5 g_1(q^2) - i\sigma_{\mu\nu}\gamma_5 q^\nu g_2(q^2) - q^\mu\gamma_5 g_3(q^2)]u_{\Lambda_b}(p_{\Lambda_b}), \quad (2.39)$$

$$\langle\Lambda(p_\Lambda) \mid \bar{s}i\sigma_{\mu\nu}q^\nu(1+\gamma_5)b \mid \Lambda_b(p_{\Lambda_b})\rangle = \bar{u}_\Lambda(p_\Lambda)[\gamma_\mu f_1^T(q^2) + i\sigma_{\mu\nu}q^\nu f_2^T(q^2) + q^\mu f_3^T(q^2) + \gamma_\mu\gamma_5 g_1^T(q^2) + i\sigma_{\mu\nu}\gamma_5 q^\nu g_2^T(q^2) + q^\mu\gamma_5 g_3^T(q^2)]u_{\Lambda_b}(p_{\Lambda_b}), \quad (2.40)$$

and

$$\langle\Lambda(p_\Lambda) \mid \bar{s}(1+\gamma_5)b \mid \Lambda_b(p_{\Lambda_b})\rangle = \frac{1}{m_b}\bar{u}_\Lambda(p_\Lambda)[\not{q}f_1(q^2) + iq^\mu\sigma_{\mu\nu}q^\nu f_2(q^2) + q^2 f_3(q^2) - \not{q}\gamma_5 g_1(q^2) - iq^\mu\sigma_{\mu\nu}\gamma_5 q^\nu g_2(q^2) - q^2\gamma_5 g_3(q^2)]u_{\Lambda_b}(p_{\Lambda_b}), \quad (2.41)$$

where u_{Λ_b} and u_Λ are spinors of the initial and final baryons. By the way, $f_i^{(T)}$ and $g_i^{(T)}$, with $i = 1, 2$ and 3, are transition form factors.

Using the above transition matrix elements, we find the transition amplitude for $\Lambda_b \to \Lambda \ell^+ \ell^-$ in the TC2 model as

$$\begin{aligned}\mathcal{M}_{\rm TC2}^{\Lambda_b \to \Lambda \ell^+ \ell^-} = \frac{G_F \alpha_{em} V_{tb} V_{ts}^*}{2\sqrt{2}\pi} \{ & [\bar{u}_\Lambda(p_\Lambda)(\gamma_\mu[\mathcal{A}_1 R + \mathcal{B}_1 L] + i\sigma_{\mu\nu} q^\nu [\mathcal{A}_2 R + \mathcal{B}_2 L] \\ & + q^\mu [\mathcal{A}_3 R + \mathcal{B}_3 L]) u_{\Lambda_b}(p_{\Lambda_b})](\bar{\ell}\gamma^\mu \ell) + [\bar{u}_\Lambda(p_\Lambda)(\gamma_\mu[\mathcal{D}_1 R + \mathcal{E}_1 L] \\ & + i\sigma_{\mu\nu} q^\nu [\mathcal{D}_2 R + \mathcal{E}_2 L] + q^\mu [\mathcal{D}_3 R + \mathcal{E}_3 L]) u_{\Lambda_b}(p_{\Lambda_b})](\bar{\ell}\gamma^\mu \gamma_5 \ell) \\ & + [\bar{u}_\Lambda(p_\Lambda)(\not{q}[\mathcal{G}_1 R + \mathcal{H}_1 L] + i q^\mu \sigma_{\mu\nu} q^\nu [\mathcal{G}_2 R + \mathcal{H}_2 L] \\ & + q^2 [\mathcal{G}_3 R + \mathcal{H}_3 L]) u_{\Lambda_b}(p_{\Lambda_b})](\bar{\ell}\ell) + [\bar{u}_\Lambda(p_\Lambda)(\not{q}[\mathcal{K}_1 R + \mathcal{S}_1 L] \\ & + i q^\mu \sigma_{\mu\nu} q^\nu [\mathcal{K}_2 R + \mathcal{S}_2 L] + q^2 [\mathcal{K}_3 R + \mathcal{S}_3 L]) u_{\Lambda_b}(p_{\Lambda_b})](\bar{\ell}\gamma_5 \ell)\}, \end{aligned} \tag{2.42}$$

where $R = (1 + \gamma_5)/2$ and $L = (1 - \gamma_5)/2$. The calligraphic coefficients are defined as

$$\begin{aligned} \mathcal{A}_1 &= (f_1 - g_1)\tilde{C}_9^{\rm eff} - 2m_b \frac{1}{q^2}(f_1^T + g_1^T)\tilde{C}_7^{\rm eff}, & \mathcal{G}_1 &= \frac{1}{m_b}(f_1 - g_1) C_{Q_1}, \\ \mathcal{A}_2 &= \mathcal{A}_1(1 \to 2), & \mathcal{G}_2 &= \mathcal{G}_1(1 \to 2), \\ \mathcal{A}_3 &= \mathcal{A}_1(1 \to 3), & \mathcal{G}_3 &= \mathcal{G}_1(1 \to 3), \\ \mathcal{B}_1 &= \mathcal{A}_1(g_1 \to -g_1; g_1^T \to -g_1^T), & \mathcal{H}_1 &= \mathcal{G}_1(g_1 \to -g_1), \\ \mathcal{B}_2 &= \mathcal{B}_1(1 \to 2), & \mathcal{H}_2 &= \mathcal{H}_1(1 \to 2), \\ \mathcal{B}_3 &= \mathcal{B}_1(1 \to 3), & \mathcal{H}_3 &= \mathcal{H}_1(1 \to 3), \\ \mathcal{D}_1 &= (f_1 - g_1)\tilde{C}_{10}, & \mathcal{K}_1 &= \frac{1}{m_b}(f_1 - g_1) C_{Q_2}, \\ \mathcal{D}_2 &= \mathcal{D}_1(1 \to 2), & \mathcal{K}_2 &= \mathcal{K}_1(1 \to 2), \\ \mathcal{D}_3 &= \mathcal{D}_1(1 \to 3), & \mathcal{K}_3 &= \mathcal{K}_1(1 \to 3), \\ \mathcal{E}_1 &= \mathcal{D}_1(g_1 \to -g_1), & \mathcal{S}_1 &= \mathcal{K}_1(g_1 \to -g_1), \\ \mathcal{E}_2 &= \mathcal{E}_1(1 \to 2), & \mathcal{S}_2 &= \mathcal{S}_1(1 \to 2), \\ \mathcal{E}_3 &= \mathcal{E}_1(1 \to 3), & \mathcal{S}_3 &= \mathcal{S}_1(1 \to 3). \end{aligned} \tag{2.43}$$

III. PHYSICAL OBSERVABLES

In this section, we calculate some physical observables such as the differential decay width, the differential branching ratio, the branching ratio and the lepton forward-backward asymmetry for the decay channel under consideration.

A. The differential decay width

In the present subsection, using the above-mentioned amplitude, we find the differential decay rate in terms of form factors in the full theory in the TC2 model as

$$\frac{d^2\Gamma}{d\hat{s}dz}(z, \hat{s}) = \frac{G_F^2 \alpha_{em}^2 m_{\Lambda_b}}{16384\pi^5} |V_{tb}V_{ts}^*|^2 v\sqrt{\lambda(1, r, \hat{s})}[\mathcal{T}_0(\hat{s}) + \mathcal{T}_1(\hat{s}) z + \mathcal{T}_2(\hat{s}) z^2], \tag{3.1}$$

where $v = \sqrt{1 - \frac{4m_\ell^2}{q^2}}$ is the lepton velocity, $\lambda = \lambda(1, r, \hat{s}) = (1 - r - \hat{s})^2 - 4r\hat{s}$ is the usual triangle function with $\hat{s} = q^2/m_{\Lambda_b}^2$, $r = m_\Lambda^2/m_{\Lambda_b}^2$, $z = \cos\theta$, and θ is the angle between momenta of the lepton l^+ and the Λ_b in the center of mass of leptons. The calligraphic $\mathcal{T}_0(\hat{s})$, $\mathcal{T}_1(\hat{s})$ and $\mathcal{T}_2(\hat{s})$ functions are obtained as

$$\begin{aligned}\mathcal{T}_0(\hat{s}) &= 32m_\ell^2 m_{\Lambda_b}^4 \hat{s}(1+r-\hat{s})(|\mathcal{D}_3|^2+|\mathcal{E}_3|^2) + 64m_\ell^2 m_{\Lambda_b}^3(1-r-\hat{s})\,\mathrm{Re}[\mathcal{D}_1^*\mathcal{E}_3+\mathcal{D}_3\mathcal{E}_1^*] \\ &+ 64m_{\Lambda_b}^2\sqrt{r}(6m_\ell^2 - m_{\Lambda_b}^2\hat{s})\,\mathrm{Re}[\mathcal{D}_1^*\mathcal{E}_1] + 64m_\ell^2 m_{\Lambda_b}^3\sqrt{r}\{2m_{\Lambda_b}\hat{s}\,\mathrm{Re}[\mathcal{D}_3^*\mathcal{E}_3] + (1-r+\hat{s})\,\mathrm{Re}[\mathcal{D}_1^*\mathcal{D}_3+\mathcal{E}_1^*\mathcal{E}_3]\} \\ &+ 32m_{\Lambda_b}^2(2m_\ell^2+m_{\Lambda_b}^2\hat{s})\{(1-r+\hat{s})m_{\Lambda_b}\sqrt{r}\,\mathrm{Re}[\mathcal{A}_1^*\mathcal{A}_2+\mathcal{B}_1^*\mathcal{B}_2] - m_{\Lambda_b}(1-r-\hat{s})\,\mathrm{Re}[\mathcal{A}_1^*\mathcal{B}_2+\mathcal{A}_2^*\mathcal{B}_1] \\ &- 2\sqrt{r}(\mathrm{Re}[\mathcal{A}_1^*\mathcal{B}_1] + m_{\Lambda_b}^2\hat{s}\,\mathrm{Re}[\mathcal{A}_2^*\mathcal{B}_2])\} + 8m_{\Lambda_b}^2\{4m_\ell^2(1+r-\hat{s}) + m_{\Lambda_b}^2[(1-r)^2-\hat{s}^2]\}(|\mathcal{A}_1|^2+|\mathcal{B}_1|^2) \\ &+ 8m_{\Lambda_b}^4\{4m_\ell^2[\lambda+(1+r-\hat{s})\hat{s}] + m_{\Lambda_b}^2\hat{s}[(1-r)^2-\hat{s}^2]\}(|\mathcal{A}_2|^2+|\mathcal{B}_2|^2) - 8m_{\Lambda_b}^2\{4m_\ell^2(1+r-\hat{s}) \\ &- m_{\Lambda_b}^2[(1-r)^2-\hat{s}^2]\}(|\mathcal{D}_1|^2+|\mathcal{E}_1|^2) + 8m_{\Lambda_b}^5\hat{s}v^2\{-8m_{\Lambda_b}\hat{s}\sqrt{r}\,\mathrm{Re}[\mathcal{D}_2^*\mathcal{E}_2] + 4(1-r+\hat{s})\sqrt{r}\,\mathrm{Re}[\mathcal{D}_1^*\mathcal{D}_2+\mathcal{E}_1^*\mathcal{E}_2] \\ &- 4(1-r-\hat{s})\,\mathrm{Re}[\mathcal{D}_1^*\mathcal{E}_2+\mathcal{D}_2^*\mathcal{E}_1] + m_{\Lambda_b}[(1-r)^2-\hat{s}^2](|\mathcal{D}_2|^2+|\mathcal{E}_2|^2)\} - 8m_{\Lambda_b}^4\{4m_\ell[(1-r)^2 \\ &- \hat{s}(1+r)]\mathrm{Re}[\mathcal{D}_1^*\mathcal{K}_1+\mathcal{E}_1^*\mathcal{S}_1] + (4m_\ell^2 - m_{\Lambda_b}^2\hat{s})[(1-r)^2-\hat{s}(1+r)](|\mathcal{G}_1|^2+|\mathcal{H}_1|^2) + 4m_{\Lambda_b}^2\sqrt{r}\hat{s}^2(4m_\ell^2 - m_{\Lambda_b}^2\hat{s}) \\ &\times \mathrm{Re}[\mathcal{G}_3^*\mathcal{H}_3]\} - 8m_{\Lambda_b}^5\hat{s}\{2\sqrt{r}(4m_\ell^2 - m_{\Lambda_b}^2\hat{s})(1-r+\hat{s})\,\mathrm{Re}[\mathcal{G}_1^*\mathcal{G}_3+\mathcal{H}_1^*\mathcal{H}_3] + 4m_\ell\sqrt{r}(1-r+\hat{s}) \\ &\times \mathrm{Re}[\mathcal{D}_1^*\mathcal{K}_3+\mathcal{E}_1^*\mathcal{S}_3+\mathcal{D}_3^*\mathcal{K}_1+\mathcal{E}_3^*\mathcal{S}_1] + 4m_\ell(1-r-\hat{s})\,\mathrm{Re}[\mathcal{D}_1^*\mathcal{S}_3+\mathcal{E}_1^*\mathcal{K}_3+\mathcal{D}_3^*\mathcal{S}_1+\mathcal{E}_3^*\mathcal{K}_1] \\ &+ 2(1-r-\hat{s})(4m_\ell^2 - m_{\Lambda_b}^2\hat{s})\,\mathrm{Re}[\mathcal{G}_1^*\mathcal{H}_3+\mathcal{H}_1^*\mathcal{G}_3] - m_{\Lambda_b}[(1-r)^2-\hat{s}(1+r)](|\mathcal{K}_1|^2+|\mathcal{S}_1|^2)\} \\ &- 32m_{\Lambda_b}^4\sqrt{r}\hat{s}\{2m_\ell\,\mathrm{Re}[\mathcal{D}_1^*\mathcal{S}_1+\mathcal{E}_1^*\mathcal{K}_1] + (4m_\ell^2 - m_{\Lambda_b}^2\hat{s})\,\mathrm{Re}[\mathcal{G}_1^*\mathcal{H}_1]\} + 8m_{\Lambda_b}^6\hat{s}^2\{4\sqrt{r}\,\mathrm{Re}[\mathcal{K}_1^*\mathcal{S}_1] \\ &+ 2m_{\Lambda_b}\sqrt{r}(1-r+\hat{s})\,\mathrm{Re}[\mathcal{K}_1^*\mathcal{K}_3+\mathcal{S}_1^*\mathcal{S}_3] + 2m_{\Lambda_b}(1-r-\hat{s})\,\mathrm{Re}[\mathcal{K}_1^*\mathcal{S}_3+\mathcal{S}_1^*\mathcal{K}_3] \\ &- (4m_\ell^2 - m_{\Lambda_b}^2\hat{s})(1+r-\hat{s})(|\mathcal{G}_3|^2+|\mathcal{H}_3|^2) - 4m_\ell(1+r-\hat{s})\,\mathrm{Re}[\mathcal{D}_3^*\mathcal{K}_3+\mathcal{E}_3^*\mathcal{S}_3] \\ &- 8m_\ell\sqrt{r}\,\mathrm{Re}[\mathcal{D}_3^*\mathcal{S}_3+\mathcal{E}_3^*\mathcal{K}_3]\} + 8m_{\Lambda_b}^8\hat{s}^3\{(1+r-\hat{s})(|\mathcal{K}_3|^2+|\mathcal{S}_3|^2) + 4\sqrt{r}\,\mathrm{Re}[\mathcal{K}_3^*\mathcal{S}_3]\}, \end{aligned} \tag{3.2}$$

$$\begin{aligned}\mathcal{T}_1(\hat{s}) &= -32m_{\Lambda_b}^4 m_\ell\sqrt{\lambda}v(1-r)\,\mathrm{Re}(\mathcal{A}_1^*\mathcal{G}_1+\mathcal{B}_1^*\mathcal{H}_1) - 16m_{\Lambda_b}^4\hat{s}v\sqrt{\lambda}\{2\,\mathrm{Re}(\mathcal{A}_1^*\mathcal{D}_1) - 2\,\mathrm{Re}(\mathcal{B}_1^*\mathcal{E}_1) \\ &+ 2m_{\Lambda_b}\,\mathrm{Re}(\mathcal{B}_1^*\mathcal{D}_2 - \mathcal{B}_2^*\mathcal{D}_1 + \mathcal{A}_2^*\mathcal{E}_1 - \mathcal{A}_1^*\mathcal{E}_2) + 2m_{\Lambda_b}m_\ell\,\mathrm{Re}(\mathcal{A}_1^*\mathcal{H}_3 + \mathcal{B}_1^*\mathcal{G}_3 - \mathcal{A}_2^*\mathcal{H}_1 - \mathcal{B}_2^*\mathcal{G}_1)\} \\ &+ 32m_{\Lambda_b}^5\hat{s}v\sqrt{\lambda}\{m_{\Lambda_b}(1-r)\,\mathrm{Re}(\mathcal{A}_2^*\mathcal{D}_2 - \mathcal{B}_2^*\mathcal{E}_2) + \sqrt{r}\,\mathrm{Re}(\mathcal{A}_2^*\mathcal{D}_1 + \mathcal{A}_1^*\mathcal{D}_2 - \mathcal{B}_2^*\mathcal{E}_1 - \mathcal{B}_1^*\mathcal{E}_2) \\ &- \sqrt{r}m_\ell\,\mathrm{Re}(\mathcal{A}_1^*\mathcal{G}_3 + \mathcal{B}_1^*\mathcal{H}_3 + \mathcal{A}_2^*\mathcal{G}_1 + \mathcal{B}_2^*\mathcal{H}_1)\} + 32m_{\Lambda_b}^6 m_\ell\sqrt{\lambda}v\hat{s}^2\,\mathrm{Re}(\mathcal{A}_2^*\mathcal{G}_3 + \mathcal{B}_2^*\mathcal{H}_3), \end{aligned} \tag{3.3}$$

and

$$\begin{aligned}\mathcal{T}_2(\hat{s}) &= -8m_{\Lambda_b}^4 v^2\lambda(|\mathcal{A}_1|^2+|\mathcal{B}_1|^2+|\mathcal{D}_1|^2+|\mathcal{E}_1|^2) \\ &+ 8m_{\Lambda_b}^6\hat{s}v^2\lambda(|\mathcal{A}_2|^2+|\mathcal{B}_2|^2+|\mathcal{D}_2|^2+|\mathcal{E}_2|^2). \end{aligned} \tag{3.4}$$

We integrate Eq. (3.1) over z in the interval $[-1, 1]$ in order to obtain the differential decay width only, with respect to $\hat{s}$. Consequently, we get

$$\frac{d\Gamma}{d\hat{s}}(\hat{s}) = \frac{G_F^2\alpha_{em}^2 m_{\Lambda_b}}{8192\pi^5}|V_{tb}V_{ts}^*|^2 v\sqrt{\lambda}\left[\mathcal{T}_0(\hat{s}) + \frac{1}{3}\mathcal{T}_2(\hat{s})\right]. \tag{3.5}$$

B. The differential branching ratio

In this subsection, we analyze the differential branching ratio of the transition under consideration in different lepton channels. For this aim, using the differential decay width in Eq. (3.5), we discuss the variation of the differential branching ratio with respect to q^2 and other related parameters. Thus, we need some of the input parameters presented in Tables I and II.

We also use the typical values $m_{\pi_t^0} = m_{h_t^0} = 300$ GeV, $m_{\pi_t^+} = 450$ GeV, $M_{Z'} = 1500$ GeV, $\varepsilon = 0.08$ and $K_1 = 0.4$ in our numerical calculations [12].

For other input parameters, we need the form factors calculated via light cone QCD sum rules in full theory [31]. The fit function for $f_1, f_2, f_3, g_1, g_2, g_3, f_2^T, f_3^T, g_2^T$ and g_3^T is given by [31] (for an alternative parametrization of form factors see [32])

$$f_i^{(T)}(q^2)[g_i^{(T)}(q^2)] = \frac{a}{(1-\frac{q^2}{m_{\rm fit}^2})} + \frac{b}{(1-\frac{q^2}{m_{\rm fit}^2})^2}, \tag{3.6}$$

where a, b and $m_{\rm fit}^2$ are the fit parameters presented in Table III. The values of the corresponding form factors at $q^2 = 0$ are also presented in Table III. In addition, the fit function of the form factors f_1^T and g_1^T is given by [31]

TABLE I. The values of some of the input parameters used in the numerical analysis. The quarks masses are in the $\overline{\text{MS}}$ scheme [30].

Input parameters	Values
m_e	0.51×10^{-3} GeV
m_μ	0.1056 GeV
m_τ	1.776 GeV
m_c	1.275 GeV
m_b	4.18 GeV
m_t	160 GeV
m_W	80.4 GeV
m_Z	91.2 GeV
m_{Λ_b}	5.620 GeV
m_Λ	1.1156 GeV
τ_{Λ_b}	1.425×10^{-12} s
$\hbar$	6.582×10^{-25} GeV s
G_F	1.17×10^{-5} GeV^{-2}
α_{em}	1/137
$\lvert V_{tb} V_{ts}^* \rvert$	0.041

$$f_1^T(q^2)[g_1^T(q^2)] = \frac{c}{\left(1 - \frac{q^2}{m_{\text{fit}}'^2}\right)} - \frac{c}{\left(1 - \frac{q^2}{m_{\text{fit}}''^2}\right)^2}, \quad (3.7)$$

where c, $m_{\text{fit}}'^2$ and $m_{\text{fit}}''^2$ are the fit parameters whose values we present, together with the values of the corresponding form factors at $q^2 = 0$, in Table IV.

The dependencies of the differential branching ratio on q^2, $m_{\pi_t^+}$ and $M_{Z'}$ in the cases of μ and τ leptons in both the SM and TC2 model are shown in Figs. 1–6. In each figure we show the dependencies of the differential branching ratio on different observables for both central values of the form factors (left panel) and for the form factors with their uncertainties (right panel). Note that the results for the case of e are very close to those of μ, so we do not present the results for e in our figures. We also depict the recent experimental results on the differential branching ratio in the μ channel provided by the CDF [1]

TABLE II. The values of some of the input parameters related to the TC2 model used in the numerical analysis [12].

Input parameters	Values
$m_{\pi_t^0}$	(200–500) GeV
$m_{\pi_t^+}$	(350–600) GeV
$m_{h_t^0}$	(200–500) GeV
$M_{Z'}$	(1200–1800) GeV
F_π	50 GeV
ε	(0.06–0.1)
K_1	(0.3–1)

TABLE III. The fit parameters a, b and m_{fit}^2 appear in the fit function of the form factors f_1, f_2, f_3, g_1, g_2, g_3, f_2^T, f_3^T, g_2^T and g_3^T together with the values of the corresponding form factors at $q^2 = 0$ in the full theory for $\Lambda_b \to \Lambda \ell^+ \ell^-$ decay [31].

	a	b	m_{fit}^2	Form factors at $q^2 = 0$
f_1	−0.046	0.368	39.10	0.322 ± 0.112
f_2	0.0046	−0.017	26.37	-0.011 ± 0.004
f_3	0.006	−0.021	22.99	-0.015 ± 0.005
g_1	−0.220	0.538	48.70	0.318 ± 0.110
g_2	0.005	−0.018	26.93	-0.013 ± 0.004
g_3	0.035	−0.050	24.26	-0.014 ± 0.005
f_2^T	−0.131	0.426	45.70	0.295 ± 0.105
f_3^T	−0.046	0.102	28.31	0.056 ± 0.018
g_2^T	−0.369	0.664	59.37	0.294 ± 0.105
g_3^T	−0.026	−0.075	23.73	-0.101 ± 0.035

and LHCb [2] Collaborations in Fig. 1. From this figure, we conclude that

(i) for both lepton channels, there are considerable differences between predictions of the SM and TC2 model on the differential branching ratio with respect to q^2, $m_{\pi_t^+}$ and $M_{Z'}$ when the central values of the form factors are considered.

(ii) Although the swept regions in both models coincide somewhere, adding the uncertainties of the form factors cannot totally eliminate the differences between the two models' predictions on the differential branching ratio.

(iii) In the case of the differential branching ratio in terms of q^2 in the μ channel (Fig. 1), the experimental data from the CDF and LHCb Collaborations are, overall, close to the SM predictions for $q^2 \leq 16$ GeV^2. When $q^2 > 16$ GeV^2 the experimental data lie in the common region swept by the SM and TC2 model.

To better compare the results, we depict the numerical values of the differential branching ratio at different values of q^2 in its allowed region for all lepton channels and both the SM and TC2 model in Tables V, VI, and VII. We also present the experimental data in the μ channel, provided by the CDF [1] and LHCb [2]

TABLE IV. The fit parameters c, $m_{\text{fit}}'^2$ and $m_{\text{fit}}''^2$ in the fit function of the form factors f_1^T and g_1^T together with the values of the related form factors at $q^2 = 0$ in the full theory for $\Lambda_b \to \Lambda \ell^+ \ell^-$ decay [31].

	c	$m_{\text{fit}}'^2$	$m_{\text{fit}}''^2$	Form factors at $q^2 = 0$
f_1^T	−1.191	23.81	59.96	0 ± 0.0
g_1^T	−0.653	24.15	48.52	0 ± 0.0

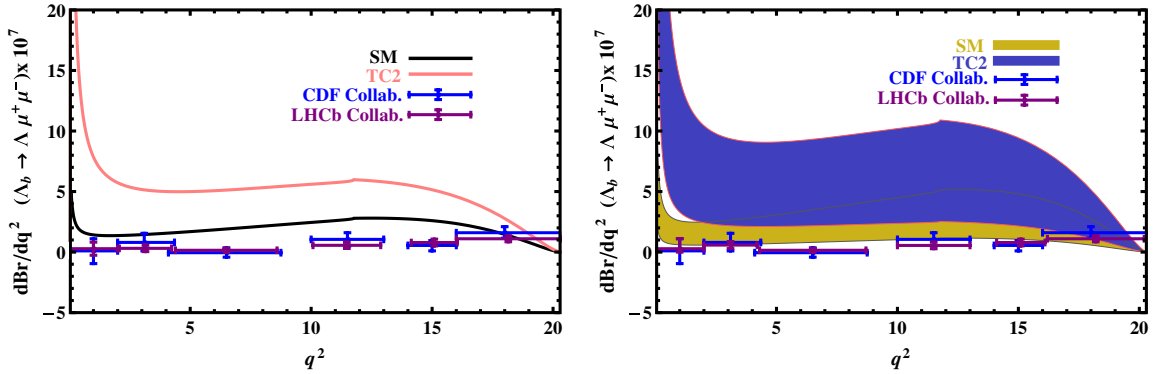

FIG. 1 (color online). The dependence of the differential branching ratio (in GeV^{-2} units) on q^2 (GeV^2) for the $\Lambda_b \to \Lambda\mu^+\mu^-$ decay channel in the SM and TC2 model using the central values of the form factors (left panel) and the form factors with their uncertainties (right panel). The recent experimental results by CDF [1] and LHCb [2] are also presented in both figures.

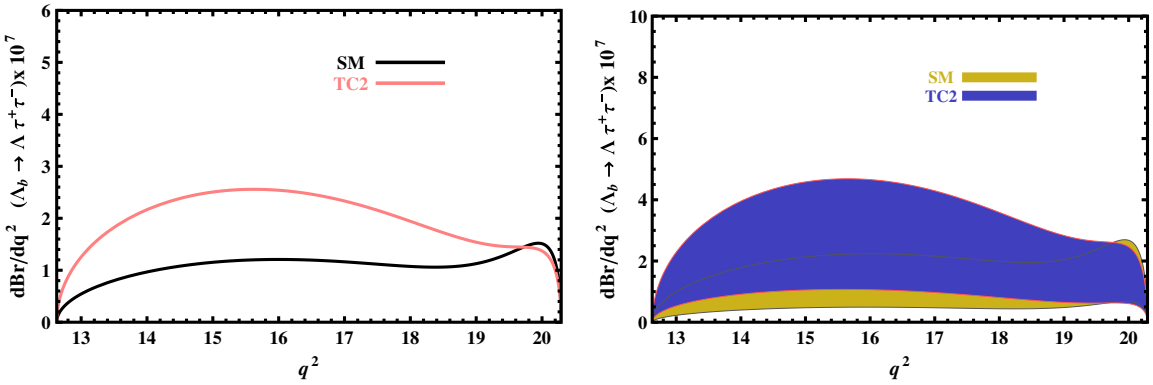

FIG. 2 (color online). The dependence of the differential branching ratio (in GeV^{-2} units) on q^2 (GeV^2) for the $\Lambda_b \to \Lambda\tau^+\tau^-$ decay channel in the SM and TC2 model using the central values of the form factors (left panel) and the form factors with their uncertainties (right panel).

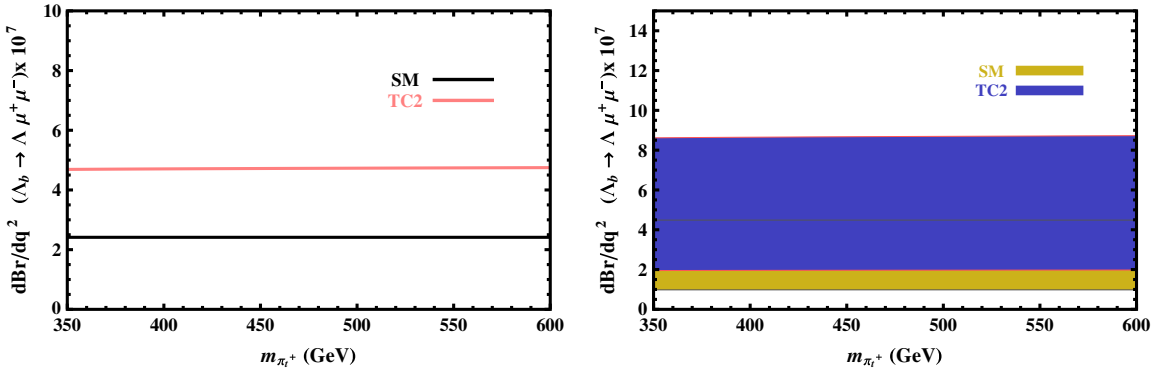

FIG. 3 (color online). The dependence of the differential branching ratio (in GeV^{-2} units) on $m_{\pi_t^+}$ for the $\Lambda_b \to \Lambda\mu^+\mu^-$ decay channel in the SM and TC2 model using the central values of the form factors (left panel) and the form factors with their uncertainties (right panel).

Collaborations, in Table V. With a quick glance at these tables, we see that

(i) in the case of μ, the experimental data on the differential branching ratio, especially those provided by the CDF Collaboration, coincide with or are close to the intervals predicted by the SM in all ranges of q^2. Within the errors, the results of TC2 are consistent with the data from the CDF Collaboration in the intervals

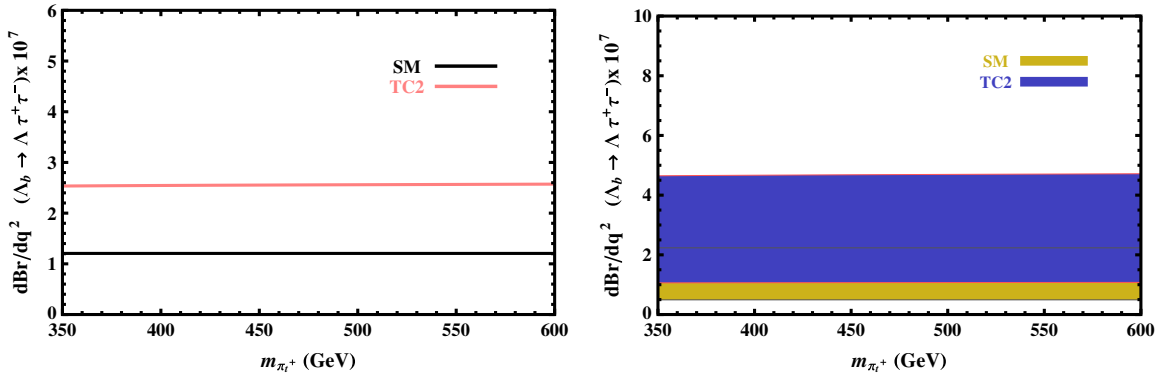

FIG. 4 (color online). The same as Fig. 3 but for the $\Lambda_b \to \Lambda\tau^+\tau^-$ decay channel.

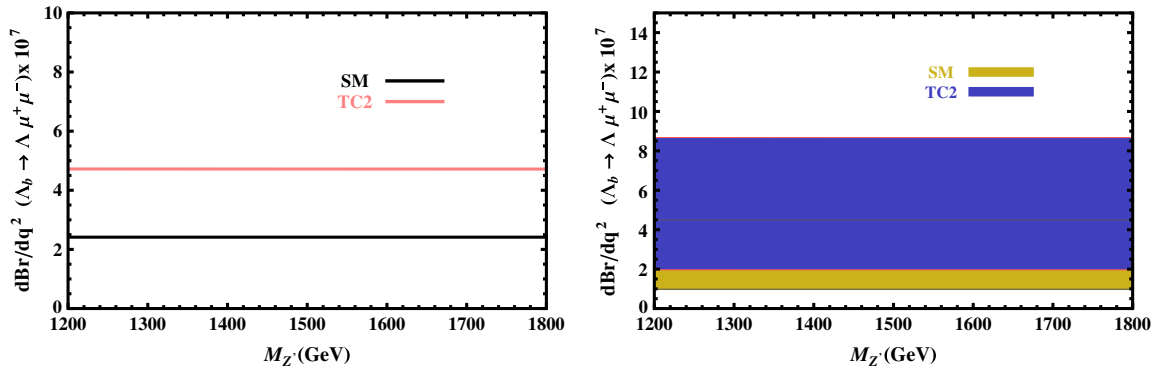

FIG. 5 (color online). The dependence of the differential branching ratio (in GeV^{-2} units) on $M_{Z'}$ for the $\Lambda_b \to \Lambda\mu^+\mu^-$ decay channel in the SM and TC2 model using the central values of the form factors (left panel) and the form factors with their uncertainties (right panel).

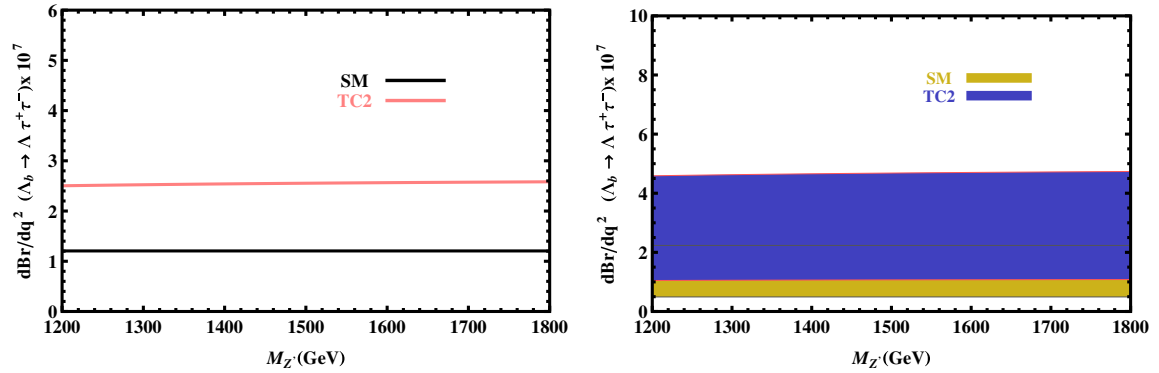

FIG. 6 (color online). The same as Fig. 5 but for the $\Lambda_b \to \Lambda\tau^+\tau^-$ decay channel.

[2.00–4.30], [10.09–12.86] and [16.00–20.30] for the q^2 and with the data from the LHCb Collaboration only for the interval [16.00–20.30] for q^2.

(ii) In all lepton channels and within the errors, the intervals predicted by the TC2 model for the differential branching ratio coincide partly with the intervals predicted by the SM approximately in all ranges of q^2.

These results show that, although central values of the theoretical results differ considerably from the experimental data, considering the errors of form factors brings the intervals predicted by theory in both models close to the experimental data, especially in the case of the SM.

C. The branching ratio

In this subsection, we calculate the values of the branching ratio of the transition under consideration both in the

TABLE V. Numerical values of the differential branching ratio in GeV^{-2} for different intervals of q^2 (GeV^2) for the $\Lambda_b \to \Lambda\mu^+\mu^-$ decay channel in the SM and TC2 model obtained using the typical values of the masses $m_{\pi_t^+} = 450$ GeV and $M_{Z'} = 1500$ GeV. We also show the experimental values of the differential branching ratio provided by the CDF [1] and LHCb [2] Collaborations.

	SM	TC2	CDF [1]	LHCb [2]
q^2	$d\mathrm{Br}/dq^2[10^{-7}]$	$d\mathrm{Br}/dq^2[10^{-7}]$	$d\mathrm{Br}/dq^2[10^{-7}]$	$d\mathrm{Br}/dq^2[10^{-7}]$
0.00–2.00	(0.60–2.58)	(3.29–14.36)	$0.15 \pm 2.01 \pm 0.05$	$0.28 \pm 0.38 \pm 0.40 \pm 0.06$
2.00–4.30	(0.61–2.65)	(2.16–9.33)	$1.84 \pm 1.66 \pm 0.59$	$0.31 \pm 0.26 \pm 0.07 \pm 0.07$
4.30–8.68	(0.80–3.48)	(2.17–9.31)	$-0.20 \pm 1.64 \pm 0.08$	$0.15 \pm 0.17 \pm 0.02 \pm 0.03$
10.09–12.86	(1.11–4.93)	(2.46–10.62)	$2.97 \pm 1.47 \pm 0.95$	$0.56 \pm 0.21 \pm 0.16 \pm 0.12$
14.18–16.00	(1.05–4.78)	(2.13–9.37)	$0.96 \pm 0.73 \pm 0.31$	$0.79 \pm 0.24 \pm 0.15 \pm 0.17$
16.00–20.30	(0.54–2.57)	(1.06–4.84)	$6.97 \pm 1.88 \pm 2.23$	$1.10 \pm 0.18 \pm 0.17 \pm 0.24$

TABLE VI. Numerical values of the differential branching ratio in GeV^{-2} for different intervals of q^2 (GeV^2) for the $\Lambda_b \to \Lambda e^+ e^-$ decay channel in the SM and TC2 model obtained using the typical values of the masses $m_{\pi_t^+} = 450$ GeV and $M_{Z'} = 1500$ GeV.

	SM	TC2
q^2	$d\mathrm{Br}/dq^2[10^{-7}]$	$d\mathrm{Br}/dq^2[10^{-7}]$
0.00–2.00	(0.60–2.59)	(3.29–14.37)
2.00–4.30	(0.61–2.65)	(2.17–9.34)
4.30–8.68	(0.80–3.49)	(2.17–9.32)
10.09–12.86	(1.11–4.94)	(2.46–10.63)
14.18–16.00	(1.05–4.78)	(2.13–9.37)
16.00–20.30	(0.54–2.57)	(1.06–4.84)

TABLE VII. Numerical values of the differential branching ratio in GeV^{-2} for different intervals of q^2 (GeV^2) for the $\Lambda_b \to \Lambda\tau^+\tau^-$ decay channel in the SM and TC2 model obtained using the typical values of the masses $m_{\pi_t^+} = 450$ GeV and $M_{Z'} = 1500$ GeV.

	SM	TC2
q^2	$d\mathrm{Br}/dq^2[10^{-7}]$	$d\mathrm{Br}/dq^2[10^{-7}]$
12.60–12.86	(0.11–0.53)	(0.28–1.22)
14.18–16.00	(0.47–2.15)	(1.05–4.61)
16.00–20.30	(0.43–1.96)	(0.77–3.46)

SM and TC2 model. For this aim, we need to multiply the total decay width by the lifetime of the initial baryon Λ_b and divide by $\hbar$. Taking into account the typical values for $m_{\pi_t^+}$ and $M_{Z'}$, we present the numerical results obtained from our calculations for both models, together with the existing experimental data provided by the CDF [1] and LHCb [2] Collaborations in Table VIII. As can be seen from this table,

(i) although the central values of the branching ratios in the TC2 model are roughly 2–3.5 times bigger than those of the SM, adding the errors of the form factors causes the intervals of the values predicted by the two models for all lepton channels to coincide.

(ii) The order of the branching ratios shows that the $\Lambda_b \to \Lambda\ell^+\ell^-$ decay can be accessible at the LHC for all leptons. As already mentioned, this decay in the μ channel has previously been observed by the CDF and LHCb Collaborations.

(iii) As is expected, the value of the branching ratio decreases by increasing the mass of the final lepton.

(iv) In the case of the μ channel, the experimental data on the branching ratio coincide with the interval predicted by the SM within errors, but these data considerably differ from the interval predicted by the TC2 model.

In order to see how the TC2 model predictions deviate from those of the SM, we plot the variations of the branching ratios on $m_{\pi_t^+}$ and $M_{Z'}$ in Figs. 7–10. From these figures we see that

(i) there are big differences between the predictions of the SM and TC2 model on the branching ratios with

TABLE VIII. Numerical values of the branching ratio of $\Lambda_b \to \Lambda\ell^+\ell^-$ for $m_{\pi_t^+} = 450$ GeV and $M_{Z'} = 1500$ GeV in the SM and TC2 model, together with the experimental data provided by the CDF [1] and LHCb [2] Collaborations.

	$\mathrm{BR}(\Lambda_b \to \Lambda e^+ e^-)[10^{-6}]$	$\mathrm{BR}(\Lambda_b \to \Lambda\mu^+\mu^-)[10^{-6}]$	$\mathrm{BR}(\Lambda_b \to \Lambda\tau^+\tau^-)[10^{-6}]$
SM	(1.81–8.06)	(1.64–7.30)	(0.34–1.51)
TC2	(6.62–29.03)	(4.55–19.81)	(0.63–2.77)
CDF [1]	...	$1.73 \pm 0.42 \pm 0.55$	...
LHCb [2]	...	$0.96 \pm 0.16 \pm 0.13 \pm 0.21$	...

respect to $m_{\pi_t^+}$ and $M_{Z'}$ when the central values of the form factors are considered.

(ii) The branching ratios remain approximately unchanged when the masses of $m_{\pi_t^+}$ and $M_{Z'}$ are varied in the regions presented in the figures for both leptons.

(iii) Adding the uncertainties of the form factors, we end up with intersections between the swept regions of the two models, but cannot totally eliminate the differences between the two models' predictions.

D. The FBA

The present subsection embraces our analysis of the lepton forward-backward asymmetry ($\mathcal{A}_{\rm FB}$) in both the SM and TC2 model. The FBA is one of the most important tools to investigate the NP beyond the SM, and it is defined as

$$\mathcal{A}_{\rm FB}(\hat{s}) = \frac{\int_0^1 \frac{d\Gamma}{d\hat{s}dz}(z,\hat{s})dz - \int_{-1}^0 \frac{d\Gamma}{d\hat{s}dz}(z,\hat{s})dz}{\int_0^1 \frac{d\Gamma}{d\hat{s}dz}(z,\hat{s})dz + \int_{-1}^0 \frac{d\Gamma}{d\hat{s}dz}(z,\hat{s})dz}. \tag{3.8}$$

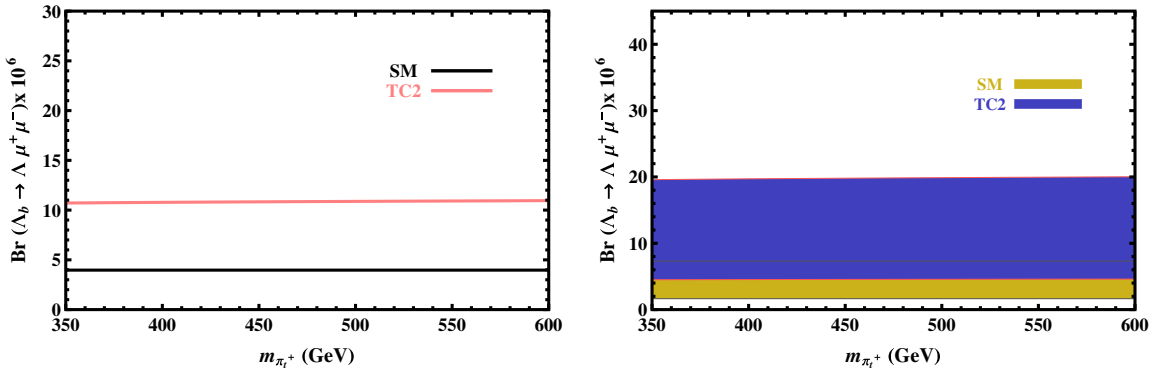

FIG. 7 (color online). The dependence of the branching ratio on $m_{\pi_t^+}$ for the $\Lambda_b \to \Lambda\mu^+\mu^-$ decay channel in the SM and TC2 model using the central values of the form factors (left panel) and the form factors with their uncertainties (right panel).

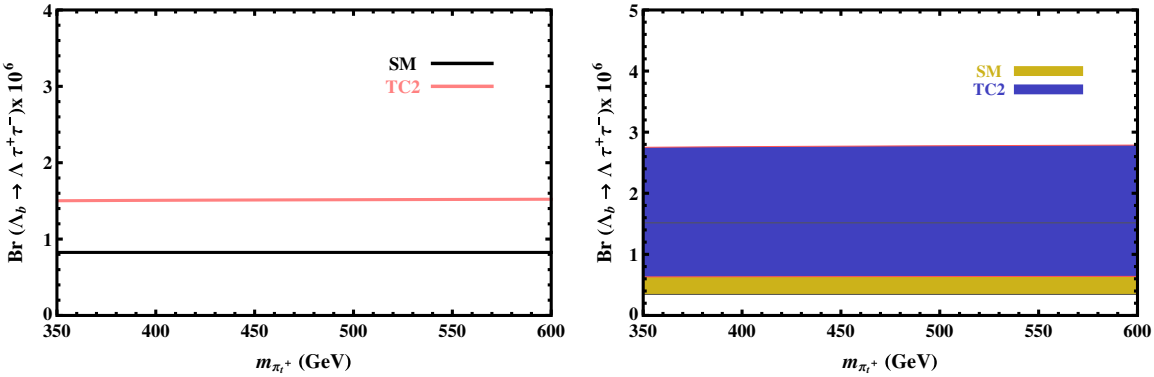

FIG. 8 (color online). The same as Fig. 7 but for the $\Lambda_b \to \Lambda\tau^+\tau^-$ transition.

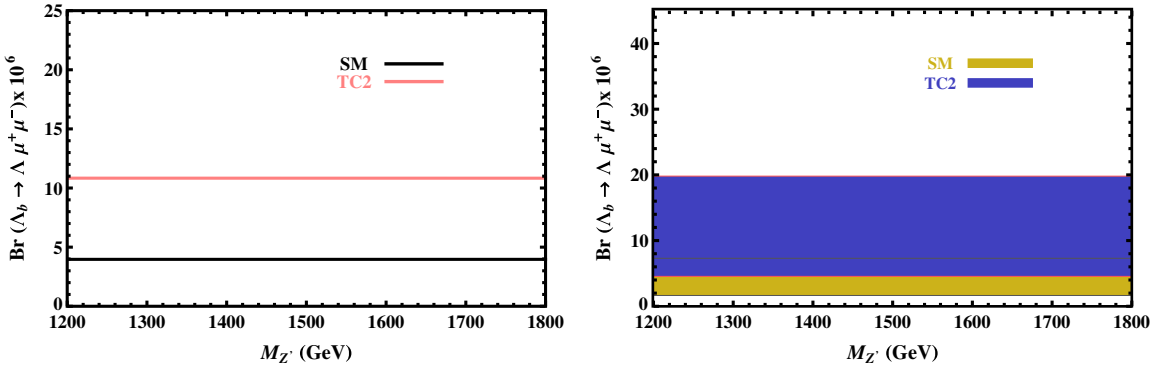

FIG. 9 (color online). The same as Fig. 7 but with respect to $M_{Z'}$.

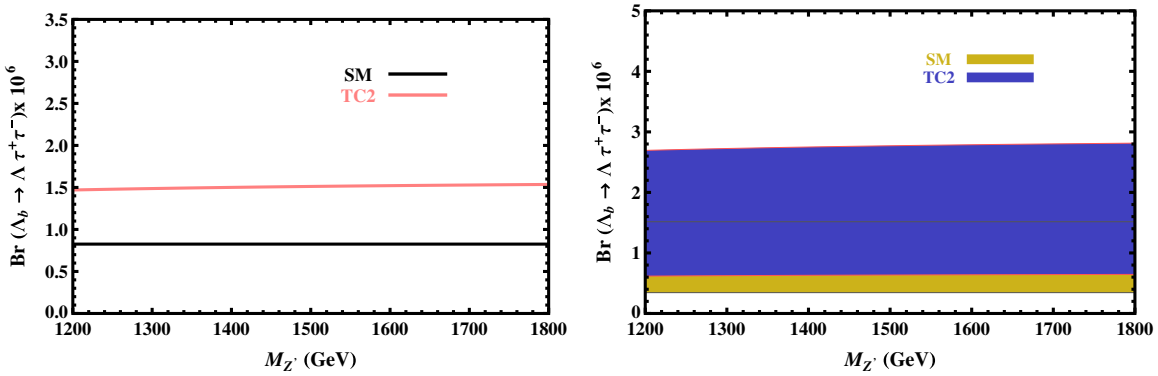

FIG. 10 (color online). The same as Fig. 9 but for the $\Lambda_b \to \Lambda \tau^+ \tau^-$ transition.

The dependencies of the FBA on q^2, $m_{\pi_t^+}$ and $M_{Z'}$ for the decay under consideration in both the μ and τ channels are depicted in Figs. 11–16. A quick glance at these figures leads to the following results:

(i) The effects of the uncertainties of the form factors on $\mathcal{A}_{\rm FB}$ are smaller compared to the differential branching ratio and the branching ratio discussed in the previous figures.

(ii) In Fig. 11, where the dependence of $\mathcal{A}_{\rm FB}$ on q^2 in the μ channel is discussed, we see considerable differences between the two models' predictions at lower values of q^2 in the left and right panels. At higher values of q^2, the two models have approximately the same predictions. In the τ case (Fig. 12), the two models have roughly the same results.

(iii) In the case of $\mathcal{A}_{\rm FB}$ in terms of $m_{\pi_t^+}$ and the μ channel, the uncertainties of the form factors end up in some common regions between the two models' predictions. In the case of the τ channel, the difference between the two models' results exists even when considering the uncertainties of the form factors.

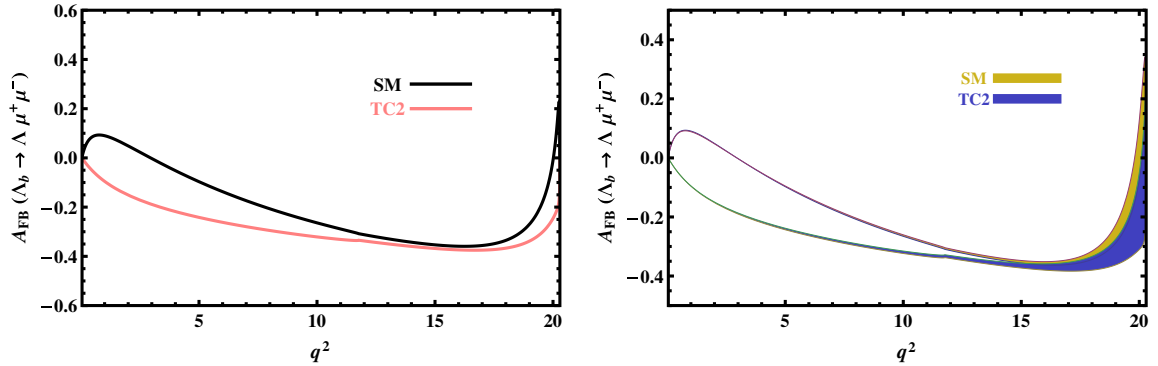

FIG. 11 (color online). The dependence of the FBA on q^2 for the $\Lambda_b \to \Lambda \mu^+ \mu^-$ decay channel in the SM and TC2 model using the central values of the form factors (left panel) and the form factors with their uncertainties (right panel).

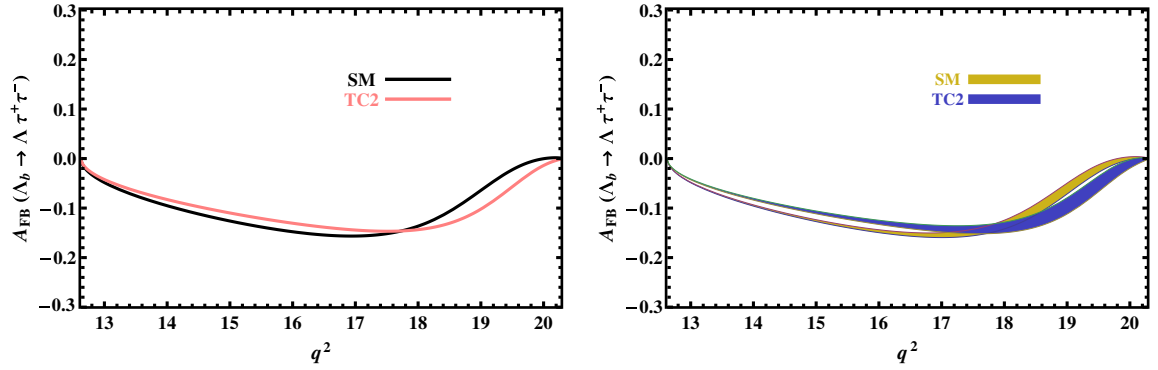

FIG. 12 (color online). The same as Fig. 11 but for the $\Lambda_b \to \Lambda \tau^+ \tau^-$ decay channel.

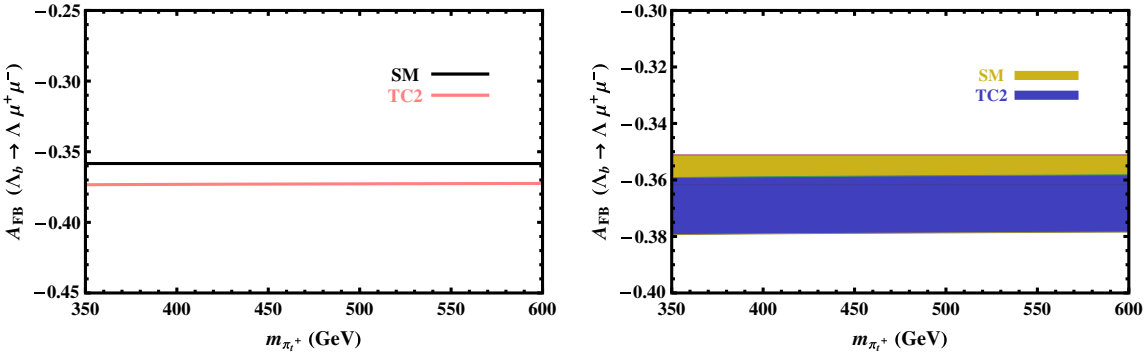

FIG. 13 (color online). The same as Fig. 11 but with respect to $m_{\pi_t^+}$.

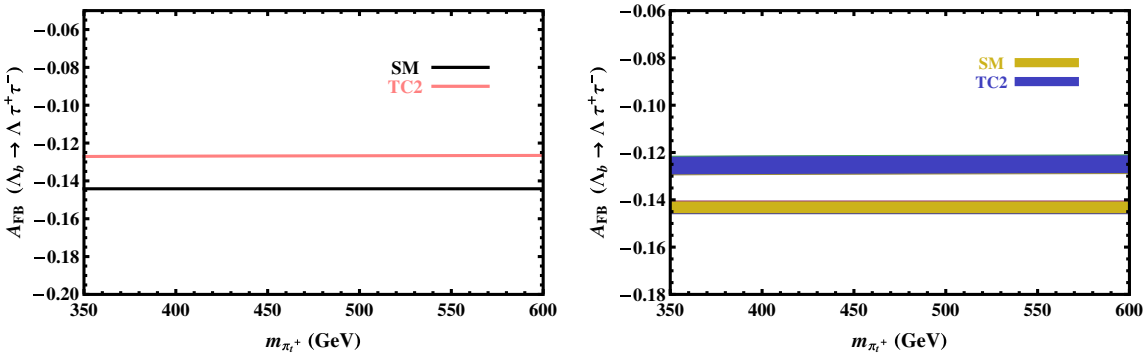

FIG. 14 (color online). The same as Fig. 13 but for the $\Lambda_b \to \Lambda\tau^+\tau^-$ decay channel.

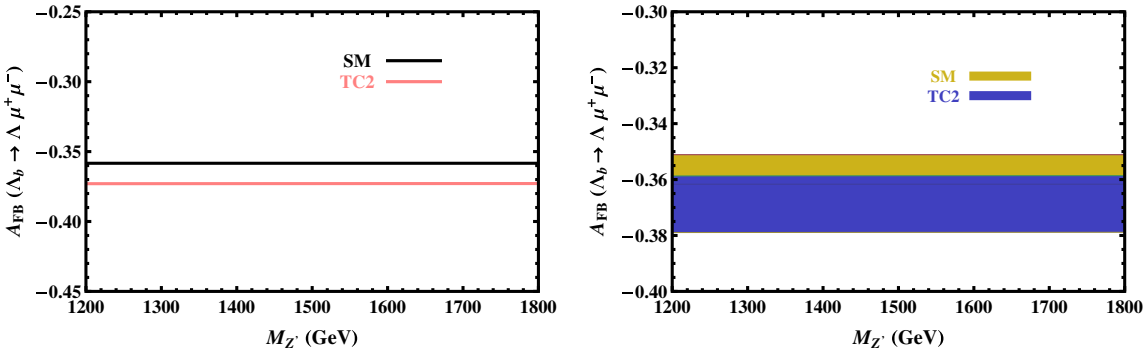

FIG. 15 (color online). The same as Fig. 11 but with respect to $M_{Z'}$.

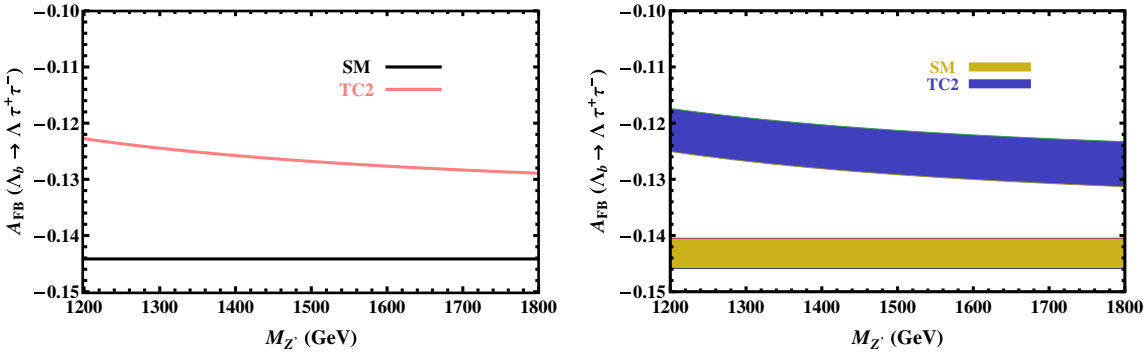

FIG. 16 (color online). The same as Fig. 15 but for the $\Lambda_b \to \Lambda\tau^+\tau^-$ decay channel.

(iv) In the case of $\mathcal{A}_{\rm FB}$ on $M_{Z'}$ and the μ channel, we see a small difference between the SM and TC2 model predictions when the central values of the form factors are considered. Taking into account the uncertainties of the form factors causes some intersections between the two models' predictions. In the case of τ (Fig. 16), we see considerable discrepancies between the two models' predictions which cannot be eliminated by the uncertainties of the form factors.

(v) $\mathcal{A}_{\rm FB}$ is sensitive to q^2 for both leptons. $\mathcal{A}_{\rm FB}$ is also sensitive to $M_{Z'}$ only for the case of τ. However, this quantity remains roughly unchanged with respect to changes in $m_{\pi_t^+}$ for both lepton channels, as well as with respect to $M_{Z'}$ only for the μ channel.

IV. CONCLUSION

In the present work, we have performed a comprehensive analysis of the baryonic FCNC $\Lambda_b \to \Lambda \ell^+ \ell^-$ channel, both in the SM and TC2 scenarios. In particular, we discussed the sensitivity of the differential branching ratio, the branching ratio and the lepton FBA on q^2 and the model parameters $m_{\pi_t^+}$ and $M_{Z'}$ using the form factors calculated via light cone QCD sum rules as the main input. We saw overall considerable differences between the two models' predictions, which cannot be totally eliminated by the uncertainties of the form factors as the main sources of errors. However, the existing experimental data provided by the CDF and LHCb Collaborations in the case of the differential branching ratios with respect to q^2 are very close to the SM results, approximately in all ranges of q^2 when the errors of the form factors are considered. Only in some intervals of q^2 do the experimental data on the differential branching ratio lie in the intervals predicted by the TC2 model within the errors. From the experimental side, we think we should have more data on different physical quantities defining the decay under consideration at different lepton channels, as well as different baryonic and mesonic processes. This will help us in searching for NP effects, especially those in the TC2 model, as an alternative EWSB scenario to the Higgs mechanism.

ACKNOWLEDGMENTS

We would like to thank Y. Erkuzu for her contribution in the early stages of the calculations.

[1] T. Aaltonen *et al.* (CDF Collaboration), Phys. Rev. Lett. **107**, 201802 (2011).
[2] LHCb Collaboration, arXiv:1306.2577.
[3] ATLAS Collaboration, Phys. Lett. B **716**, 1 (2012).
[4] CMS Collaboration, Phys. Lett. B **716**, 30 (2012).
[5] R. K. Kaul, Rev. Mod. Phys. **55**, 449 (1983).
[6] C. T. Hill, Phys. Lett. B **345**, 483 (1995).
[7] K. Lane and E. Eichten, Phys. Lett. B **352**, 382 (1995).
[8] D. Kominis, Phys. Lett. B **358**, 312 (1995).
[9] Z. Xiao, W. Li, L. Guo, and G. Lu, Eur. Phys. J. C **18**, 681 (2001).
[10] Z. Xiao and L. Guo, Commun. Theor. Phys. **40**, 77 (2003).
[11] W. Liu, C.-X. Yue, and H.-D. Yang, Phys. Rev. D **79**, 034008 (2009).
[12] L.-X. Lü, X.-Q. Yang, and Z.-C. Wang, J. High Energy Phys. 07 (2012) 157.
[13] K. Lane, Phys. Lett. B **433**, 96 (1998).
[14] C. T. Hill and E. H. Simmons, Phys. Rep. **381**, 235 (2003); **390**, 553(E) (2004).
[15] G. Cvetic, Rev. Mod. Phys. **71**, 513 (1999).
[16] G. Buchalla, G. Burdman, C. T. Hill, and D. Kominis, Phys. Rev. D **53**, 5185 (1996).
[17] H.-J. He and C.-P. Yuan, Phys. Rev. Lett. **83**, 28 (1999).
[18] G. Burdman, Phys. Rev. Lett. **83**, 2888 (1999).
[19] C. T. Hill, Report No. FERMILAB-CONF-97-032-T.
[20] G. Buchalla, A. J. Buras, and M. E. Lautenbacher, Rev. Mod. Phys. **68**, 1125 (1996).
[21] G. Bobeth, A. J. Buras, F. Krüger, and J. Urban, Nucl. Phys. **B630**, 87 (2002).
[22] W. Altmannshofer, P. Ball, A. Bharucha, A. J. Buras, D. M. Straub, and M. Wick, J. High Energy Phys. 01 (2009) 019.
[23] A. Ghinculov, T. Hurth, G. Isidori, and Y. P. Yao, Nucl. Phys. **B685**, 351 (2004).
[24] A. J. Buras, M. Misiak, M. Mnz, and S. Pokorski, Nucl. Phys. **B424**, 374 (1994).
[25] M. Misiak, Nucl. Phys. **B393**, 23 (1993); **B439**, 461 (1995).
[26] A. J. Buras and M. Muenz, Phys. Rev. D **52**, 186 (1995).
[27] A. J. Buras, arXiv:hep-ph/9806471.
[28] Z. Xiao, C.-D. Lü, and W. Huo, Phys. Rev. D **67**, 094021 (2003).
[29] C.-X. Yue, J. Zhang, and W. Liu, Nucl. Phys. **B832**, 342 (2010).
[30] J. Beringer *et al.* (Particle Data Group), Phys. Rev. D **86**, 010001 (2012).
[31] T. M. Aliev, K. Azizi, and M. Savci, Phys. Rev. D **81**, 056006 (2010).
[32] T. Feldmann and M. W. Y. Yip, Phys. Rev. D **85**, 014035 (2012); **86**, 079901(E) (2012).